SLAC-PUB-10939
January 2005

MS346, MFT

Applications of Synchrotron X-rays in Microelectronics Industry Research

Jean L. Jordan-Sweet, Christophe Detavernier[a], Christian Lavoie, Patricia M. Mooney

IBM T.J. Watson Research Center, P.O. Box 218, Yorktown Heights, NY 10598

and Michael F. Toney[b]

IBM Almaden Research Center, 650 Harry Road, San Jose, CA 95120

Abstract

The high flux and density of x-rays produced at synchrotrons provide the microelectronics industry with a powerful probe of the structure and behavior of a wide array of solid materials that are being developed for use in devices of the future. They also are of great use in determining why currently-used materials and processes sometimes fail.

This paper describes the X20 x-ray beamline facility operated by IBM at the National Synchrotron Light Source, and presents a series of three industry challenges and results that illustrate the variety of techniques used and problems addressed. The value of this research ranges from solving short-term, technically-specific problems to increasing our academic understanding of materials in general. Techniques discussed include high-resolution diffraction, time-resolved diffraction, texture measurements, and grazing-incidence diffraction.

PACS 61.10-i, 68.55.Jk, 68.60.Dv, 81.07-Bc

Keywords: microelectronics materials; x-ray diffraction; synchrotron; nickel silicide; strained silicon; nanoparticles

[a] Permanent address: Department of Solid State Physics, Ghent University, 9000 Gent, Belgium

[b] Permanent address: Stanford Synchrotron Radiation Laboratory, Stanford Linear Accelerator, Menlo Park, CA 94025

Work supported in part by the Department of Energy Contract DE-AC02-76SF00515

Send proofs to: Jean Jordan-Sweet phone 631-344-8581
NSLS 535A fax 631-344-2823
Brookhaven National Laboratory email JLJS@US.IBM.COM
Upton, NY 11973

Introduction

Increases in the speed and efficiency of computer chips can no longer continue on the path set by Moore's Law through geometric scaling alone[1,2]. The smallest Complementary Metal Oxide Semiconductor (CMOS) transistor feature sizes have decreased to the nanoscale and barrier films are no more than several atomic layers thick. Chip manufacturers must rely increasingly on innovative device designs and new materials and processes for continued improvements. This in turn drives the need for scientists and engineers to find tools that can help them understand the structure and behavior of materials in configurations and situations that are close to those used in the manufacture of microelectronic devices.

The x-rays produced at synchrotrons are an ideal tool for determining the crystalline structure, thickness, and surface and interface morphology of thin films and small structures used in making chips. The wavelength is on the same scale as lattice planes of metals, semiconductors and insulators. The flux and brightness are high enough to yield measurable signals from thin, small or low-density samples. Sometimes measurements are made in a time-resolved mode during annealing, or mechanical or electrical stressing, or other processing. Finally, the energy tunability allows one to use anomalous effects, fluorescence signals,

Extended X-ray Absorption Fine Structure (EXAFS), and other techniques that are not available from laboratory x-ray sources.

The X20 Beamlines at the NSLS

IBM runs three beamlines at the National Synchrotron Light Source (NSLS) which were designed for x-ray diffraction and versatility in experimental station configuration [3]. X20A and C have energy-tunable double-crystal Si(111) or Ge(111) monochromators and 1:1 toroidal focusing mirrors. The beam size at the sample is less than 1mm FWHM, and the flux ranges up to a maximum of ~$5x10^{11}$ photons/sec at 8-9 keV. The monochromator in X20C was designed alternatively to house synthetic multilayers, which have a band pass of about 1.5% and yield a factor of about 100 times more flux[4]. Beamline X20B incorporates a fixed-energy bent-flag Si(111) monochromator which produces $2x10^{11}$ photons/sec at 17.43 keV. The beam profile at the sample position is ~0.63 mm (horizontal) by 6 mm (vertical).

Three experimental station configurations are commonly switched in and out several times a year. X20A has a standard four-circle Huber diffractometer, or can be configured for microbeam diffraction. X20C also has a standard Huber diffractometer, which can be configured for time-resolved diffraction with a special chamber and fast linear detector[5]. X20B can be outfitted with a standard diffractometer or a cryomagnet on a modified diffractometer.

Example 1: Thermal stability of strained silicon CMOS

One recent innovation for increasing the speed of Field Effect Transistors is to make the carrier channel out of strained silicon. Strained Si CMOS devices, made by the epitaxial growth of a 10-30 nm-thick strained Si layer on a relaxed $Si_{1-x}Ge_x$ buffer layer on Si(001) show significantly increased electron and hole mobility[6]. However, a variety of standard device-

fabrication processes, such as ion-implantation and gate oxidation, require annealing temperatures of up to 1000ºC. These temperatures may induce relaxation in the strained Si and interdiffusion at the Si/SiGe interface. Using Ultra-High Vacuum Chemical Vapor Deposition (UHVCVD)-grown film samples to model these devices, changes during thermal annealing in N_2 at 1000ºC for 5, 30, and 300 seconds were measured using high-resolution x-ray diffraction (XRD)[7]. Samples were measured that varied in Ge content from 19 to 30% and Si layer thickness from 7 to 30 nm. Figure 1 shows a radial scan taken in the region of the Si and SiGe (004) peaks, with and without a 21 nm-thick strained Si cap layer on $Si_{0.72}Ge_{0.28}$. The difference curve yields the intensity from the strained Si layer, and the position of the main peak reveals the strain while the period of associated fringes gives the thickness. Figure 2a plots the change in layer thickness for samples having different $Si_{1-x}Ge_x$ alloy composition and initial layer thickness. These results show some interdiffusion, but no real dependence upon composition or initial thickness. Figure 2b shows the increase in strain relaxation relative to the initial strain for two Si layer thicknesses. The greater relaxation of the thicker film agrees with theory[6,8]. In conclusion, high-resolution XRD using a synchrotron enables one to measure very thin films and distinguish between lattice bending or mosaic and lattice parameter changes which relate to strain.

Example 2: New metal silicides for transistor contacts

CMOS transistors have historically incorporated metal silicide materials as low-resistivity contacts between the gate, source and drain, and the vias which connect them to metal wiring in the chip. In the 1990s $TiSi_2$ was the silicide of choice, to be replaced by $CoSi_2$ in current manufacturing. Both of these are formed by a nucleation-limited phase transformation from a high-resistivity phase, and have limitations for future use[9]. NiSi is a candidate for the

next generation of transistors. It follows a diffusion-controlled process, and can be formed on many different substrates, at lower temperature and with less Si consumption, and in very small dimensions[9]. The Ni-Si binary alloy phase diagram is quite complex and it is important to understand which phases are formed under different conditions such as thermal annealing ramp rate, substrate type, dopants, ambient environment, surface cleaning procedure, *etc*. The time-resolved XRD setup at X20C is ideal for rapid measuring of phase transformations for a wide array of processing conditions and sample types [5]. In addition to providing diffraction data over about 14 degrees in 2θ, the system collects optical light scattering to sense surface morphology changes on the 0.5 and 5.0 μm length scales, and four-point probe resistance[10].

Figure 3 shows a contour plot of the diffracted intensity versus temperature during a 3ºC/sec thermal anneal of 15nm Ni on polycrystalline Si[11]. Also shown are curves depicting the resistance and light scattering. One can see the formation of a number of metal-rich phases around 300ºC, followed by formation and persistence of the desired low-resistance NiSi phase between 400 and 800ºC. The rapid rise of the light scattering curves at a lower temperature than that for the $NiSi_2$ phase formation indicates that roughening and agglomeration limit the thermal processing window for this silicide. This morphological instability worsens as the films get thinner. A method that extends the temperature envelope for the NiSi phase is to add Pt as an alloying element[9]. Pt is not miscible in $NiSi_2$ and increases the transformation temperature to $NiSi_2$. Its presence also changes the texture and grain size in the NiSi film.

The texture of these films plays an important role in how stable the phases are to agglomeration and transformation. During routine pole figure analyses (maps of orientations of grains in χ and φ), a new type of texture was discovered and dubbed “axiotaxy”[12]. Figure 4 illustrates the three standard types of texture in films: 1) powder or random, 2) fiber (all

crystallites have the same set of planes parallel to the surface but are randomly oriented around a "fiber axis" normal to the surface), and 3) epitaxy (all crystallites have a registered orientation with the substrate in all three directions). In addition, the 112 pole figure for NiSi on Si(001) is shown, which displays a completely different pattern. The arcs and circles are similar to fiber rings, but rather than having the axes normal to the substrate surface, they are at a variety of angles, with the strongest lying close to 45 degrees. Axiotaxy can be described as a one-dimensional epitaxy, consisting of a preferential orientation of grains such that there is plane alignment across the interface. Lattice planes in NiSi that have d-spacings close to those of the Si(220) substrate planes orient themselves so that the plane spacing projected onto the interface is equal to that of the Si(220) planes. Planes that have their fiber axis at 45 degrees can maintain that preferred orientation even on rough interfaces and during agglomeration. The addition of a small amount of Pt, as noted earlier, discourages agglomeration. This is partly due to the fact that the Pt increases the NiSi lattice d-spacings enough to diminish axiotaxy[13]. This is shown in Figure 5. The combination of time-resolved diffraction and texture measurements available at the synchrotron enable researchers to learn about the behavior of thin film materials and tailor compositions and process variables to produce optimized characteristics and behavior.

Example 3: FePt Nanoparticle assemblies for high-density magnetic storage media

In this last example grazing-incidence diffraction was used to measure the effect of annealing on a 3-layer $Fe_{58}Pt_{42}$ assembly[14]. Monodisperse, well-oriented ferrolectric nanoparticles are good candidate materials for ultra-high density magnetic storage media of the future, possibly up to 20 Tbits/in. The sample was made by "polymer-mediated self-assembly[15]" and consisted of 4nm nanoparticles assembled layer-by-layer at room temperature. Near-Edge X-ray Absorption Fine Structure (NEXAFS) spectroscopy showed the particles to be

partly oxidized. Grazing-incidence diffraction was performed to follow the evolution of crystalline structure as a function of annealing temperature. Figure 6 shows a sequence of diffraction curves taken after annealing to increasingly higher temperatures[14]. The as-deposited film shows the chemically disordered face-centered cubic phase. Superlattice peaks appear and grow with higher annealing temperatures, indicating the formation and ripening of the high-coercivity, chemically ordered, face-centered tetragonal $L1_0$ phase. A high degree of chemical order is obtained by 800ºC, which correlates with the highest measured coercivity. Peak broadening analysis shows that the particle size also increases. In the as-deposited assembly, the diffraction grain diameter is ~2.5 nm (the oxide shell doesn't diffract). By 800ºC it has increased to nearly 20nm. This, along with x-ray reflectivity data, indicates that the particles agglomerate at high annealing temperatures. Texture measurements showed evolution from isotropic orientation to some (001) texture, which would be desirable for recording media.

Summary

Through the description of three examples of materials issues relevant to IBM Research and the variety of techniques used to address them, this paper is intended to give a flavor of the ways that synchrotron x-rays can be used for research and development in the microelectronics industry.

Acknowledgements

This work was done in part at the National Synchrotron Light Source at Brookhaven National Laboratory, supported by DOE Contract No. DE-AC02-76CH00016.

References

[1] Emerging Research Devices, in: International Technology Roadmap for Semiconductors, 2003 Edition, Semiconductor Industry Association, Austin, Texas, 2003; http://public.itrs.net.

[2] H.-S. P. Wong, IBM J. Res. Devel. 46 (2002) 133; http://www.ibm.com/journal/rd.

[3] J.L. Jordan-Sweet, IBM J. Res. Devel., 44 (2000) 457.

[4] G.B. Stephenson, Nucl. Instr. And Meth. In Phys. Res. A266 (1988) 447.

[5] L.A. Clevenger, R.A. Roy, C. Cabral, Jr., K.L. Saenger, S. Brauer, G. Morales, K.F. Ludwig, Jr., G. Gifford, J. Bucchignano, J. Jordan-Sweet, P. DeHaven, and G.B. Stephenson, J. Mater. Res. 10 (1995) 2355.

[6] P.M. Mooney, S.J. Koester, H.J. Hovel, J.O. Chu, K.K. Chan, J.L. Jordan-Sweet, J.A. Ott, N. Klymco, and D.M. Mocuta, in:, D.G. Seilor, A.C. Diebold, T.J. Schaffner, R. McDonald, S. Zollner, R.P. Khosla, E.M. Secula (Eds.), Characterization and Metrology for ULSI Technology; 2003 International Conference, AIP, Mellvilee, New York, 2003, p. 213.

[7] P.M. Mooney, S.J. Koester, J.A. Ott, J.L. Jordan-Sweet, J.O. Chu, and K.K. Chan, Mat. Res. Soc. Symp. Proc. 686 (2002) 3.

[8] J.W. Matthews and A.E. Blakeslee, J. Cryst. Growth 32 (1976) 265.

[9] C. Lavoie, F.M. d'Heurle, C. Detavernier, C. Cabral, Jr., Microelectron. Eng. 70 (2003) 144.

[10] C. Lavoie, C. Cabral, Jr., L.A. Clevenger, J.M.E. Harper, J. Jordan-Sweet, K.L. Saenger, and F. Doany, Mater. Res. Soc. Symp. Proc., 406 (1996) 163.

[11] C. Lavoie , R. Purtell, C. Coia, C. Detavernier, P. Desjardins, J. Jordan-Sweet, C. Cabral, Jr., F.M. d'Heurle, and J.M.E. Harper, Electrochem. Soc. Symp. Proc. 2002/11 (2002) 455.

[12] C. Detavernier, A.S. Ozcan, J. Jordan-Sweet, E.A. Stach, J. Tersoff, F.M. Ross, and C. Lavoie, Nature 426 (2003) 641.

[13] C. Detavernier and C. Lavoie, Appl. Phys. Lett. 84 (2004) 3549.

[14] S. Anders, M.F. Toney, T. Thomson, R.F.C. Farrow, J.-U. Thiele, B.D. Terris, S. Sun, and C.B. Murray, J. Appl. Phys. 93 (2003) 6299.

[15] S. Sun, S. Anders, H. Hamann, J.-U. Thiele, J.E.E. Baglin, T. Thomson, E.E. Fullerton, C.B. Murray, and B.D. Terris, J. Am. Chem. Soc. 124 (2002) 2884.

Figures

[1] 004 x-ray scans taken at regions with and without the 21 nm-thick strained Si cap layer on $Si_{0.72}Ge_{0.28}$.

[2] (a) Change in strained Si layer thickness with annealing time in several samples having $Si_{1-x}Ge_x$ alloy composition and initial Si layer thickness as indicated. (b) Percent strain as a function of annealing time. Strain relaxation calculated from planar view Transmission Electron Microscopy (TEM) images is also plotted.

[3] (a) Resistance and light scattering from 0.5 and 5 μm length scales together with (b) x-ray diffraction measurements performed *in situ* during annealing (3°C/sec) of a 15 nm Ni film deposited on p-doped poly-Si.

[4] Three classical and a new type of texture for thin films: (a) powder texture (simulated for Cu powder), (b) fiber texture (Cu on SiO_2), (c) epitaxy (Cu on Si(001), HF clean), and (d) axiotaxy (NiSi(112) on Si(001)).

[5] 112 pole figure for NiSi with varying amounts of added Pt.

[6] In-plane x-ray diffraction of a 3-layer $Fe_{58}Pt_{42}$ nanoparticle assembly. The ordinate is the scattering vector Q, which has a magnitude $q = (4\pi/\lambda) \sin \theta$, where λ is the x-ray wavelength (0.12 nm here) and θ is half the scattering angle. The diffraction peaks are marked.

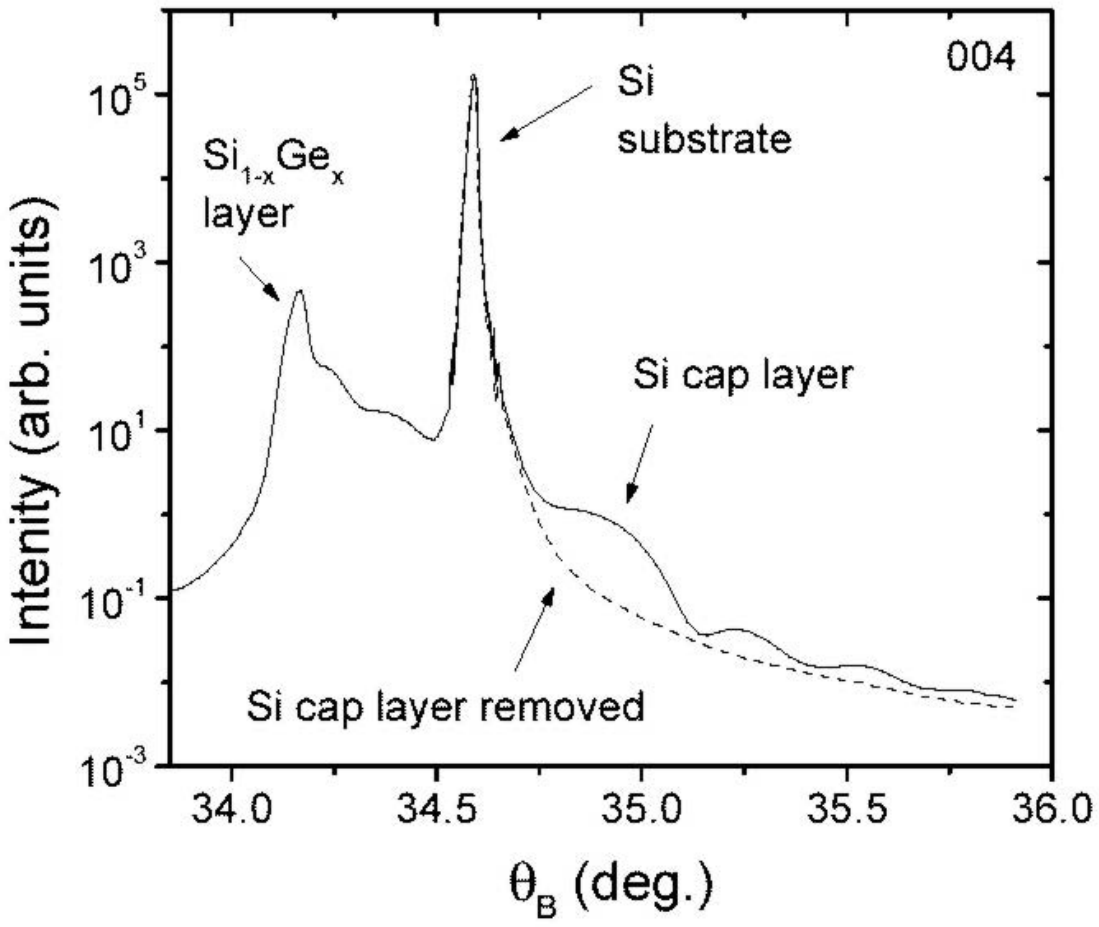
004
Si
substrate
Si$_{1-x}$Ge$_x$
layer
Si cap layer
Si cap layer removed
Intenity (arb. units)
10^5
10^3
10^1
10^{-1}
10^{-3}
34.0
34.5
35.0
35.5
36.0
θ_B (deg.)

Figure 1

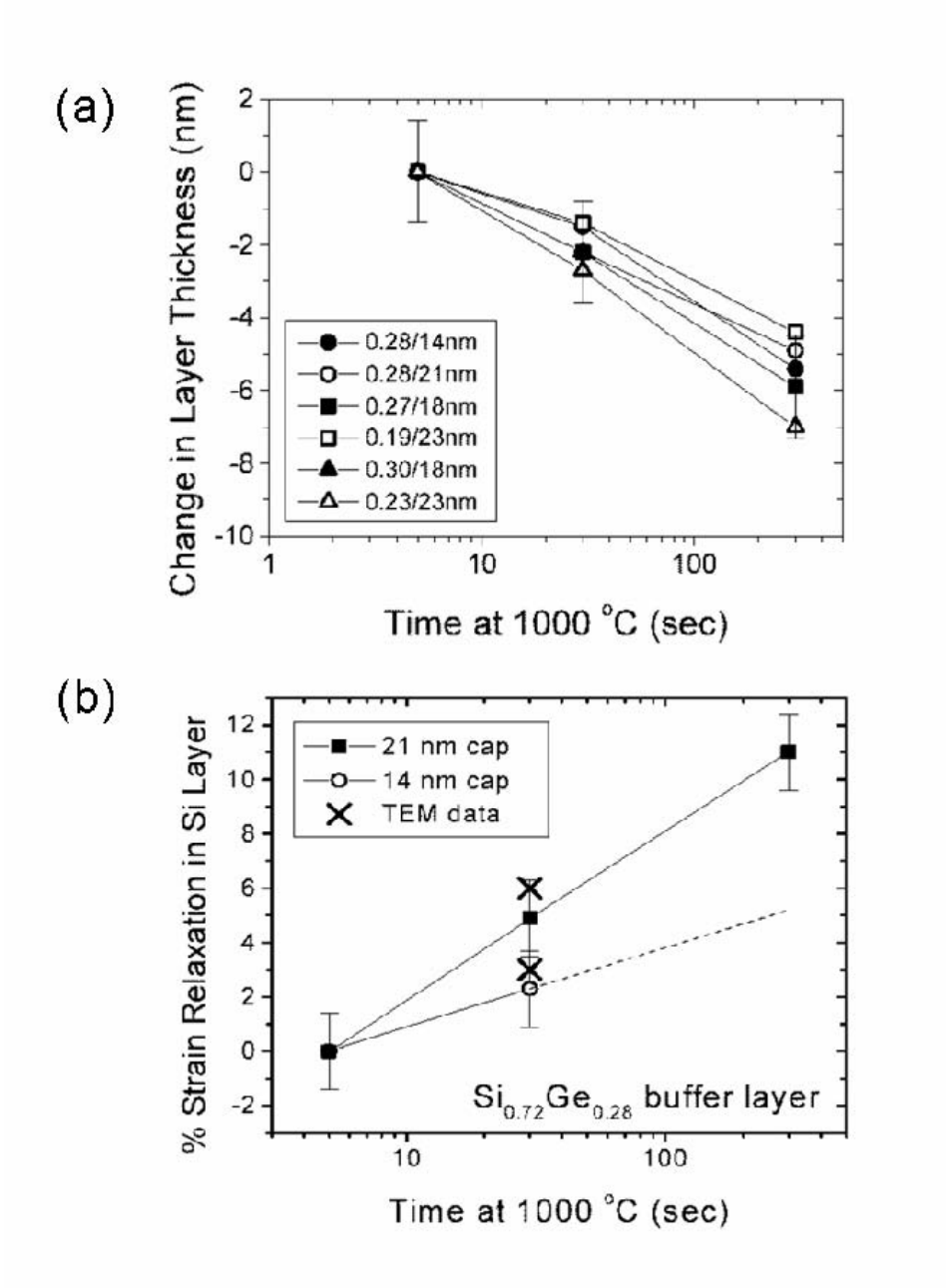
(a)
Change in Layer Thickness (nm)
2
0
-2
-4
-6
-8
-10
1
10
100
Time at 1000 °C (sec)
0.28/14nm
0.28/21nm
0.27/18nm
0.19/23nm
0.30/18nm
0.23/23nm
(b)
% Strain Relaxation in Si Layer
12
10
8
6
4
2
0
-2
10
100
Time at 1000 °C (sec)
21 nm cap
14 nm cap
TEM data
Si0.72Ge0.28 buffer layer

Figure 2

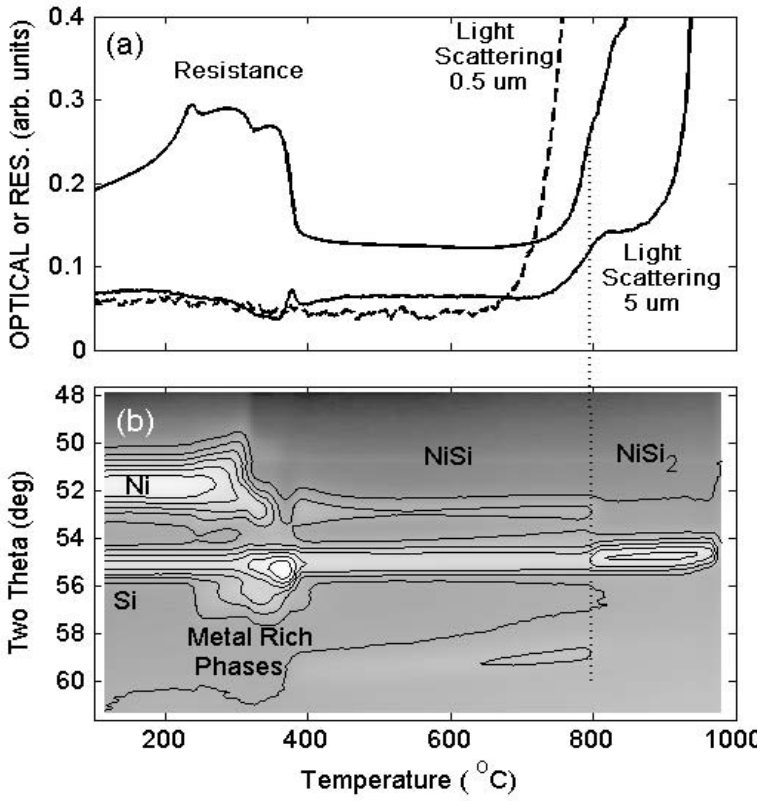
(a)
Resistance
Light Scattering 0.5 um
Light Scattering 5 um
OPTICAL or RES. (arb. units)
0.4
0.3
0.2
0.1
0
(b)
NiSi
NiSi2
Ni
Si
Metal Rich Phases
Two Theta (deg)
48
50
52
54
56
58
60
200
400
600
800
1000
Temperature (°C)

Figure 3

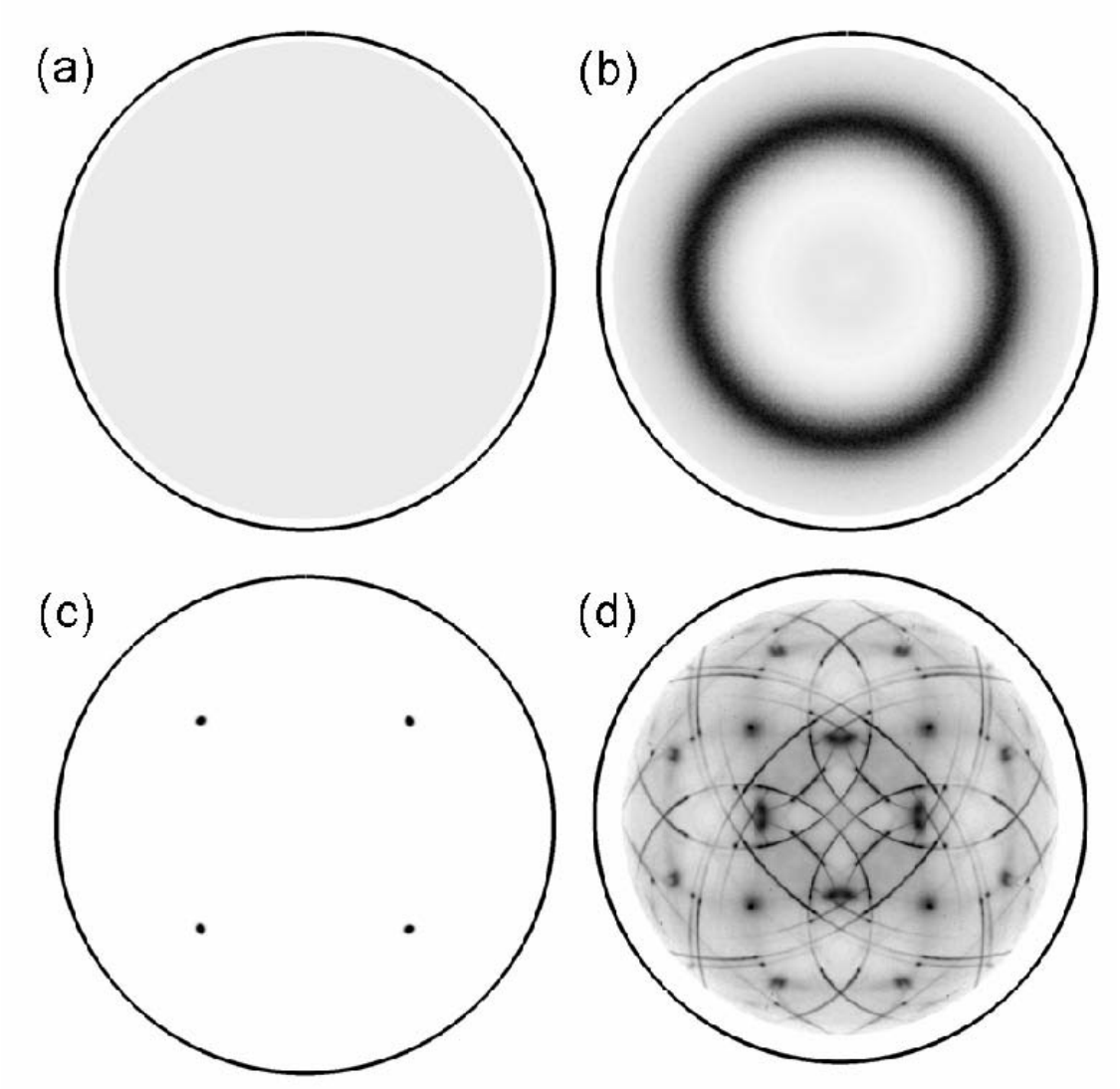

Figure 4

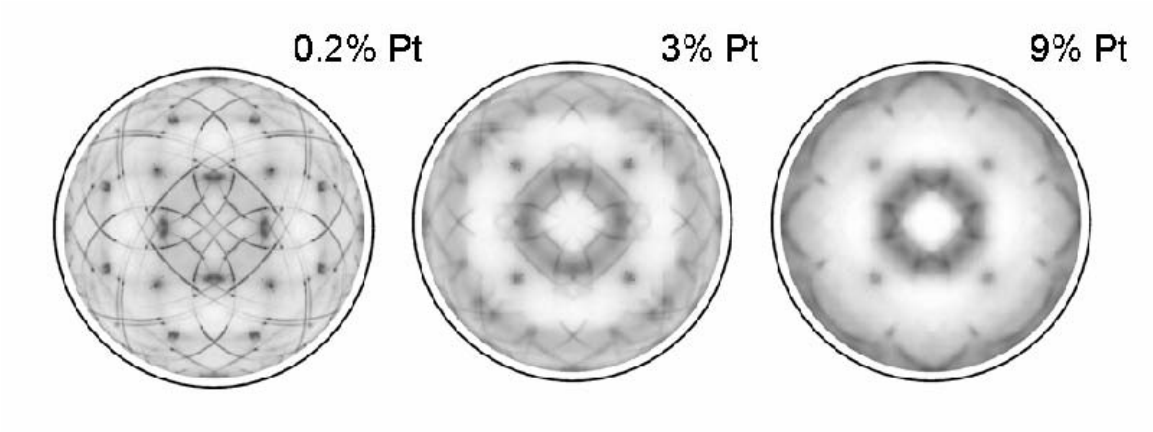

Figure 5

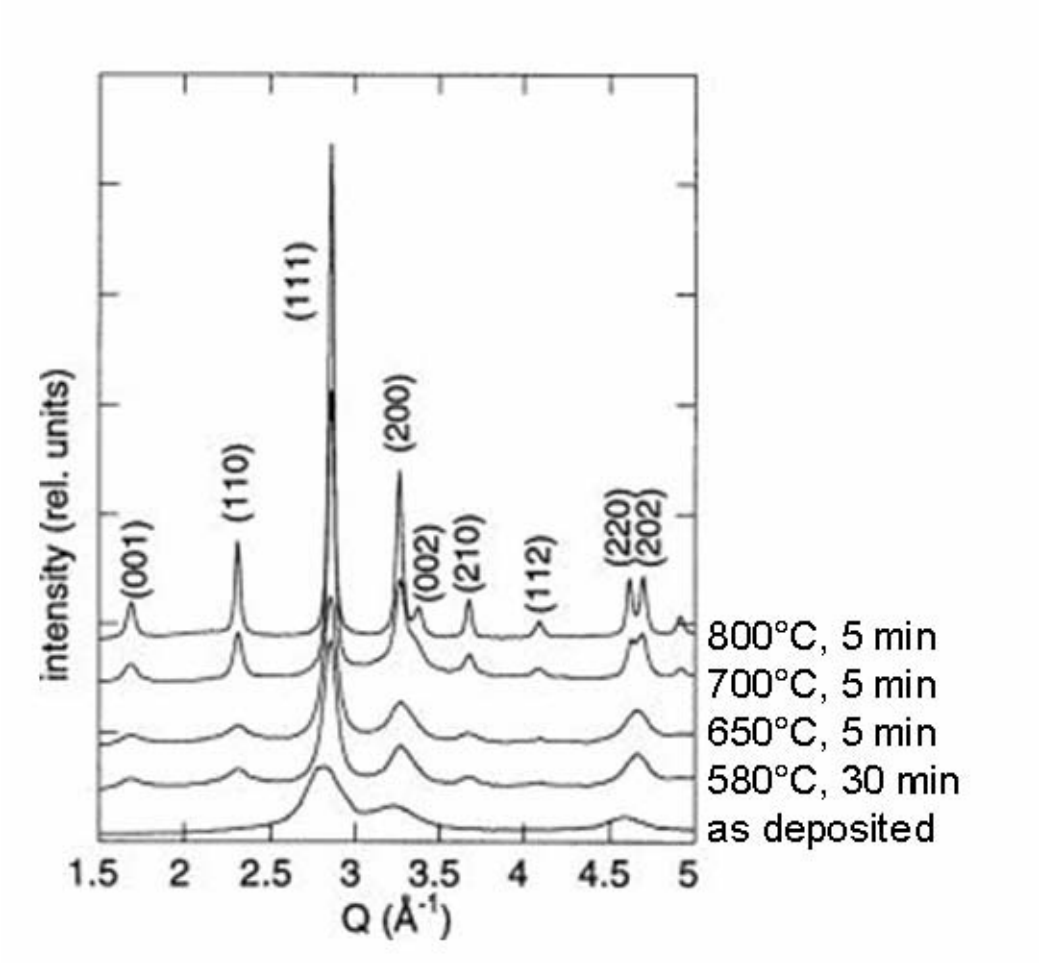
intensity (rel. units)
(001)
(110)
(111)
(200)
(002)
(210)
(112)
(220)
(202)
800°C, 5 min
700°C, 5 min
650°C, 5 min
580°C, 30 min
as deposited
1.5
2
2.5
3
3.5
4
4.5
5
Q (Å-1)

Figure 6